

Dual-Prototype Disentanglement: A Context-Aware Enhancement Framework for Time Series Forecasting

HAONAN YANG, JIANCHAO TANG*, and ZHUO LI, National University of Defense Technology, China

Time series forecasting has witnessed significant progress with deep learning. While prevailing approaches improve forecasting performance by modifying architectures or introducing novel enhancement strategies, they often fail to dynamically disentangle and leverage the complex, intertwined temporal patterns inherent in time series, thus resulting in the learning of static, averaged representations that lack context-aware capabilities. To address this, we propose the Dual-Prototype Adaptive Disentanglement framework (DPAD), a model-agnostic auxiliary method that equips forecasting models with the ability of pattern disentanglement and context-aware adaptation. Specifically, we construct a Dynamic Dual-Prototype bank (DDP), comprising a common pattern bank with strong temporal priors to capture prevailing trend or seasonal patterns, and a rare pattern bank dynamically memorizing critical yet infrequent events, and then a Dual-Path Context-aware routing (DPC) mechanism is proposed to enhance outputs with selectively retrieved context-specific pattern representations from the DDP. Additionally, we introduce a Disentanglement-Guided Loss (DGLoss) to ensure that each prototype bank specializes in its designated role while maintaining comprehensive coverage. Comprehensive experiments demonstrate that DPAD consistently improves forecasting performance and reliability of state-of-the-art models across diverse real-world benchmarks.

CCS Concepts: • **Computing methodologies** → **Artificial intelligence**.

Additional Key Words and Phrases: Time Series Forecasting, Context-Aware, Pattern Disentanglement

ACM Reference Format:

Haonan Yang, Jianchao Tang, and Zhuo Li. 2026. Dual-Prototype Disentanglement: A Context-Aware Enhancement Framework for Time Series Forecasting. 1, 1 (June 2026), 18 pages. <https://doi.org/10.1145/nnnnnnn.nnnnnnn>

1 Introduction

Time series forecasting (TSF) plays a pivotal role across numerous real-world domains, including weather forecasting [3, 45], transportation scheduling [8, 12], healthcare monitoring [34, 41], energy consumption [1, 7] and finance [5, 48]. Due to the inherent non-stationarity and dynamics, traditional methods fail to effectively model intricate patterns across different time [6, 39]. Recent advances in deep learning have demonstrated a strong capability for capturing intricate temporal dependencies in time series, making it a formidable tool for TSF [24, 38].

Prevailing research focuses on improving forecasting performance by modifying architectures [43, 44] or incorporating novel enhancement strategies [14, 20], both of which have obviously improved the ability to model intricate nonlinear patterns [28, 46]. To effectively capture complex temporal dependencies, some approaches have refined attention mechanisms [18] or redesigned MLP and CNN architectures for improved modeling of long-range and cross-channel dependencies [23, 33]. Meanwhile, some methods introduce enhancement strategies that directly encode

Authors' Contact Information: Haonan Yang, yanghaonan21@nudt.edu.cn; Jianchao Tang, tangjianchao14@nudt.edu.cn; Zhuo Li, lizhuo19@nudt.edu.cn, National University of Defense Technology, Changsha, Hunan, China.

Permission to make digital or hard copies of all or part of this work for personal or classroom use is granted without fee provided that copies are not made or distributed for profit or commercial advantage and that copies bear this notice and the full citation on the first page. Copyrights for components of this work owned by others than the author(s) must be honored. Abstracting with credit is permitted. To copy otherwise, or republish, to post on servers or to redistribute to lists, requires prior specific permission and/or a fee. Request permissions from permissions@acm.org.

© 2026 Copyright held by the owner/author(s). Publication rights licensed to ACM.

Manuscript submitted to ACM

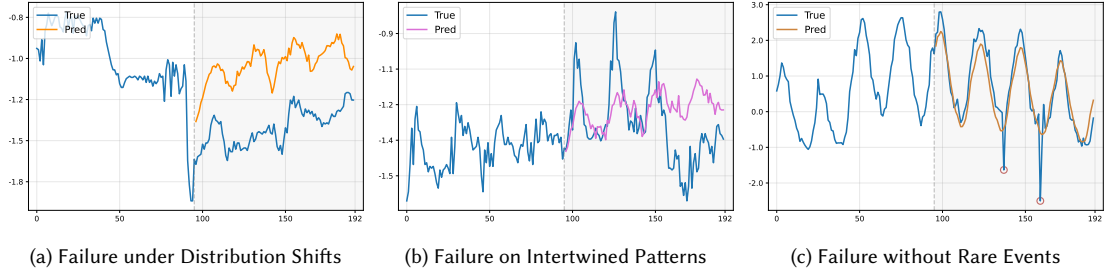


Fig. 1. Limitation of static and averaged representations in time series forecasting. We visualize three characteristic failure scenarios where some methods fall short: (a) abrupt distribution shifts, (b) intertwined complex patterns, and (c) critical rare events. These limitations motivate our proposed context-aware enhancement framework.

prior knowledge about temporal structure into the learning process, which include explicit decomposition schemes that separate trend and seasonal components, as well as techniques such as post-processing to mitigate distribution shifts [21, 25].

Despite these advancements, TSF remains challenging due to the inherent complexity in real-world time series data [40]. This complexity stems primarily from the intrinsic non-stationarity and dynamics, leading to gradual or abrupt distribution shifts over time [9]. Consequently, the learned representations by models may suffer from temporal lag. Meanwhile, time series often exhibit intertwined and complex patterns (e.g., trends, seasonality, and irregular fluctuations) [37], whose influences may vary across different periods and data [10]. In these patterns, some critical yet rare patterns occur infrequently in historical observations, resulting in long-tail distributions that models often fail to adequately memorize [21]. These inherent challenges drive existing methods toward learning averaged, static representations, thereby hindering their ability to capture complex and context-sensitive temporal dependencies [15, 29]. To better illustrate this limitation, we select three representative real-world forecasting scenarios. As shown in Figure 1, a model relying on such representations may struggle to adapt and disentangle individual patterns when confronted with distribution shifts and complex intertwined patterns. This phenomenon underscores the necessity of enhancing the model’s capability for dynamic disentanglement and adaptation to diverse temporal patterns.

To this end, we propose the Dual-Prototype Adaptive Disentanglement framework (DPAD), a novel, model-agnostic paradigm designed to overcome the limitation of static representations by endowing models with context-aware pattern disentanglement capabilities. Unlike prior works that modify the core architecture, DPAD functions as a plug-and-play auxiliary method that can be seamlessly integrated into various forecasting backbones. Specifically, our framework first establishes a learnable Dynamic Dual-Prototype bank (DDP), which comprises a common pattern bank covering prevalent and stable temporal modes, and a rare pattern bank dedicated to memorizing infrequent yet critical events. Then, a Dual-Path Context-aware routing (DPC) mechanism dynamically retrieves and activates relevant patterns from the DDP, thereby enhancing the backbone’s representation via a weighted gating strategy. Furthermore, our framework is optimized with a Disentanglement-Guided Loss (DGLoss) that jointly ensures the separation of common and rare patterns, enforces diversity among common prototypes, and maintains the distinctiveness of rare prototypes. Our contributions are summarized as follows:

- We introduce a novel context-aware enhancement framework based on dual-prototype disentanglement. Unlike existing methods, our framework equips models with the capability for context-aware and pattern disentanglement, thereby directly mitigating the inherent limitation of static representations and enhancing their ability to dynamically model intricate temporal patterns.
- We propose DPAD, a model-agnostic auxiliary framework that employs a learnable dual-prototype bank and an adaptive routing mechanism to dynamically enhance model’s prediction. A disentanglement-guided loss is further introduced to enforce effective pattern separation and preservation, which jointly optimizes the backbone and the prototype banks.
- Comprehensive experiments on multiple real-world datasets and state-of-the-art backbones demonstrate that DPAD consistently enhances forecasting performance with only negligible computational overhead.

2 Related Work

2.1 Time Series Forecasting Models

Recent years have witnessed remarkable progress in deep forecasting models, with their core advancement lying in learning more expressive temporal representations [27, 30]. Existing models can be broadly categorized by architecture into MLP-based, CNN-based, Transformer-based, and LLM-based approaches [39]. MLP-based architectures [26, 33, 47] often employ decomposition strategies and simple linear layers to capture cross-time dependencies, offering a compelling balance of efficiency and performance. CNN-based architectures [2, 16, 36] leverage hierarchical convolution structures and frequency-domain analysis [43] to model local patterns and multi-periodicity effectively. Nevertheless, both of them often struggle to capture long-term dependencies. Therefore, Transformer-based architectures [4, 17, 50] have emerged as a powerful paradigm by introducing various efficient attention mechanisms to capture global dependencies. More recently, LLM-based approaches [19, 31, 42] have explored adapting pre-trained large language models for time series forecasting, leveraging their massive parameters and in-context learning capabilities. While excelling at capturing stable, recurring patterns, these models often tend to converge to a flexible representation [35, 49]. Consequently, they struggle to adaptively disentangle representations in response to the specific context of input sequences, such as distribution shifts, intricate mixtures of patterns, or the emergence of anomalies. This inherent rigidity underscores the need for a complementary mechanism that can inject contextual adaptability into these models.

2.2 Enhancement Strategies for Time Series Forecasting

Beyond architectural innovations, several efficient and model-agnostic strategies have been proposed to enhance predictive performance. Some methods employ decomposition strategies as a strong inductive bias to guide model in handling diverse temporal patterns more effectively [11, 38]. Autoformer [44] decomposes time series into seasonal and trend components, allowing other models to handle input from a clearer perspective. TimesNet [43] learns frequency-adaptive periods in the frequency domain to explicitly model intra- and inter-period variations. Another strategy focuses on model-agnostic methods [22, 25]. RAFT [9] employs retrieval augmented generation to retrieve from historical samples, providing the model with relevant information. HCAN [32] assigns class labels for timesteps to equip models with contextual-aware capability. Furthermore, specialized loss function designs have been designed to improve robustness against distribution shifts and intricate patterns [21, 35]. DBLoss [29] decomposes both predictions and ground truth to calculate the loss for each component separately. PSLoss [15] enhances structural alignment by comparing time series at the patch level with statistical properties. While these strategies improve forecasting

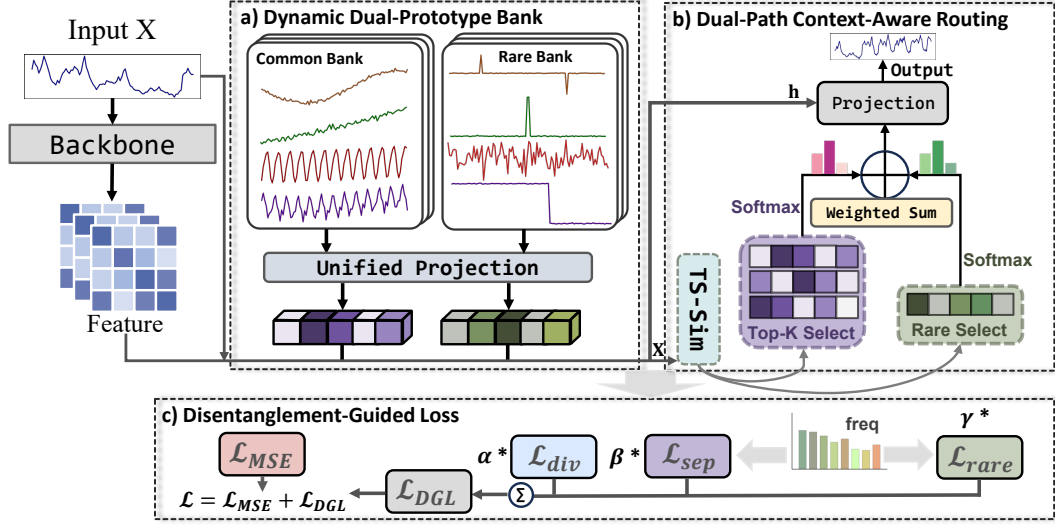


Fig. 2. The overall architecture of the DPAD framework. The framework constructs a learnable dual-prototype bank, then performs adaptive dual-path routing on the input data to retrieve relevant prototypes, and finally generates a context-aware enhancement for prediction. The entire framework is optimized under a disentanglement-guided loss.

performance, they still fail to dynamically disentangle complex, intertwined patterns in a context-aware manner. Different from them, our proposed DPAD framework introduces a learnable dual-prototype bank and adaptively fuses them through a context-aware routing mechanism, thereby enabling dynamic and interpretable enhancement of the backbone model’s representations with high efficiency.

3 Method

Time series forecasting addresses the fundamental challenge of predicting future values $Y = y_{t+1}, \dots, y_{t+h} \in \mathbb{R}^{h \times C}$ from historical observations $X = x_1, \dots, x_t \in \mathbb{R}^{t \times C}$, where h is the prediction horizon, t is the history horizon, and C is the number of variables.

3.1 Structure Overview

As illustrated in Figure 2, our proposed DPAD consists three key components: (a) Dynamic Dual-Prototype Bank (DDP) that maintains a set of common and rare pattern prototypes to explicitly disentangle different patterns and dynamically update; (b) Dual-Path Context-aware routing (DPC) that dynamically retrieves and activates relevant prototypes from DDP, in which the representation is generated by an arbitrary backbone model, and then enhances the prediction through a weighted gating strategy; (c) Disentanglement-Guided Loss (DGLoss) that jointly optimizes DDP and the backbone model through a quadruple loss formulation, which ensures both the specialization and separation of the prototypes.

3.2 Dynamic Dual-Prototype Bank

The Dynamic Dual-Prototype bank (DDP) serves as the cornerstone of our framework, designed to explicitly disentangle and memorize two distinct categories of temporal patterns: prevalent common patterns and critical yet infrequent rare

patterns. Formally, the DDP consists of two separate prototype sets: a Common Pattern Bank \mathcal{B}_c , which comprises sequences synthesized from a combination of fundamental trends and seasonal patterns, and a Rare Pattern Bank \mathcal{B}_r , dedicated to memorizing long-tailed, sudden events and some other temporal noise.

Specifically, we generate two groups of base sequences $\{\mathbf{s}_c^i\}$ and rare sequences $\{\mathbf{s}_r^j\}$ using distinct prior strategies to reflect their different pattern characteristics:

$$\mathbf{s}_c^i \sim \mathcal{GP}(0, \lambda_l K_l + \lambda_r K_r + \lambda_p K_p), \quad i = 1, \dots, M, \quad (1)$$

$$\mathbf{s}_r^j \sim \mathcal{N}(0, \sigma^2 \mathbf{I}), \quad j = 1, \dots, N, \quad (2)$$

where \mathbf{s}_c^i denotes the common sequences generated via a mixture of Gaussian Process \mathcal{GP} kernels to embed strong temporal priors, and K_l, K_r, K_p are the Linear, radial basis function (RBF), and Periodic kernel, λ_i is mixing coefficients. This strategy yields diverse yet structured prototypes that cover stable, recurring patterns such as trends, seasonality, and their mixtures, thereby providing a well-initialized basis for modeling prevalent temporal dynamics.

In contrast, \mathbf{s}_r^j is initialized from a Gaussian distribution $\mathcal{N}(0, \sigma^2 \mathbf{I})$, where σ^2 is a small variance controlling the magnitude of initialization noise. This minimal random initialization ensures that rare prototypes begin from a nearly unbiased state, allowing them to remain flexible and exclusively adapt to capture rare patterns during training, without being predisposed to common modes. Notably, all of sequence sets would be transformed into learnable parameters.

Then each generated sequence is projected into a shared D -dimensional latent space via the linear layers:

$$\mathbf{p}_c^i = \text{Proj}_c(\mathbf{s}_c^i), \quad (3)$$

$$\mathbf{p}_r^j = \text{Proj}_r(\mathbf{s}_r^j), \quad (4)$$

The resulting Common Pattern Bank \mathcal{B}_c and Rare Pattern Bank \mathcal{B}_r are defined as follows:

$$\mathcal{B}_c = \{\mathbf{p}_c^1, \mathbf{p}_c^2, \dots, \mathbf{p}_c^M\}, \quad \mathcal{B}_r = \{\mathbf{p}_r^1, \mathbf{p}_r^2, \dots, \mathbf{p}_r^N\}. \quad (5)$$

This strategy explicitly separates the modeling of common and rare patterns while keeping the prototype representation compact and adaptive. Both \mathcal{B}_c and \mathcal{B}_r are updated throughout training via the disentanglement loss described in 3.4. This allows the common prototypes to evolve toward more representative and dataset-specific stable patterns, while the rare prototypes dynamically adapt to capture and memorize infrequent yet critical temporal patterns.

3.3 Dual-Path Context-Aware Routing

Dual-Path Context-aware routing (DPC) mechanism is proposed to adaptively enhance final prediction. Given the input \mathbf{X} and its contextual representation $\mathbf{h} \in \mathbb{R}^D$ from the backbone model, our DPC dynamically retrieves and fuses relevant patterns from the DDP through a dual-path design using TS-Sim block. Specifically, we first project \mathbf{X} into the same D -dimensional latent space as the prototypes via a learnable linear projection ϕ . Then we compute the similarity scores ρ_c and ρ_r between the input \mathbf{X} and each prototype in \mathcal{B}_c and \mathcal{B}_r in the latent space:

$$\rho_c = s(\phi(\mathbf{X}), \mathcal{B}_c), \quad \rho_r = s(\phi(\mathbf{X}), \mathcal{B}_r), \quad (6)$$

Here we adopt the Pearson Correlation as the similarity measurement $s(\cdot, \cdot)$, which provides scale-invariant matching that focuses on the shape similarity of temporal patterns. We then employ a dual-path selection strategy to retrieve the most relevant prototypes:

$$\mathcal{I}_c = \arg \text{top-K}(\rho_i | 1 < i \leq K), \quad (7)$$

$$\mathcal{I}_r = \begin{cases} \arg \max(\rho_r), & \text{if } \max(\rho_r) > \epsilon \\ \emptyset, & \text{otherwise} \end{cases} \quad (8)$$

For the common bank \mathcal{B}_c , we select top-K prototypes with the highest similarity scores, forming an index set \mathcal{I}_c . Conversely, to enforce sparsity and precise memory for rare events, we select at most one prototype from the rare bank \mathcal{B}_r , with its index denoted as \mathcal{I}_r .

Then we compute adaptive weights for the selected common and rare prototypes by Softmax function:

$$\omega_c = \text{Softmax}(\rho_c[\mathcal{I}_c]/\tau), \quad \omega_r = \text{Softmax}(\rho_r[\mathcal{I}_r]/\tau), \quad (9)$$

Then the retrieved pattern contributions are then computed as weighted sums:

$$\mathbf{z}_c = \sum_{k \in \mathcal{I}_c} \omega_c^k \cdot \mathcal{B}_c[\mathcal{I}_c], \quad \mathbf{z}_r = \omega_r \cdot \mathcal{B}_r[\mathcal{I}_r], \quad (10)$$

Finally, these context-aware contributions are fused with the backbone representation \mathbf{h} through concatenation and a linear projection to produce the enhanced prediction \mathbf{Y} :

$$\mathbf{Y} = \mathbf{W}_o[\mathbf{h}; \mathbf{z}_c; \mathbf{z}_r], \quad (11)$$

This adaptive fusion mechanism thereby enhances the capability of the model to dynamically disentangle intricate temporal dependencies, which mitigates the inherent limitation of static, averaged representations.

3.4 Disentanglement-Guided Loss

To ensure the DDP learns a well-disentangled and effective representation of common and rare patterns, we propose a Disentanglement-Guided Loss (DGLoss). This loss function jointly optimizes the parameters of backbone model and the DDP by enforcing three key properties: pattern separation, rarity preservation, and common set diversity.

We first introduce the Separation Loss \mathcal{L}_{sep} to ensure a clear functional divide between the common and rare banks, preventing role confusion. Guided by pattern frequency statistics within a training batch, \mathcal{L}_{sep} dynamically encourages each bank to specialize in its respective domain:

$$\mathcal{L}_{\text{sep}} = \mathbb{E}[\omega \cdot \max(0, m - \Delta\rho) + (1 - \omega) \cdot \max(0, m + \Delta\rho)], \quad (12)$$

where $\Delta\rho$ is the difference between similarities ρ_c and ρ_r , m is a margin, and $\omega \in [0, 1]$ is a frequency weight that computed as the exponential moving average of prototypes activation frequencies across batches. Intuitively, if the input contains patterns frequently observed in recent batches, \mathcal{L}_{sep} penalizes activation of the rare bank, while for a rare input pattern, it penalizes over-reliance on the common bank.

Then we propose a Rarity Preservation Loss $\mathcal{L}_{\text{rare}}$. With the contrastive restriction, $\mathcal{L}_{\text{rare}}$ prevents the prototypes in the rare bank from being contaminated or forgotten due to common patterns, thereby ensuring their persistent memory for rare patterns:

$$\mathcal{L}_{\text{rare}} = -\frac{1}{|\mathcal{A}|} \sum_{k \in \mathcal{A}} \log\left[\frac{\exp(\frac{s_{kk}}{\tau})}{\sum_{j=1}^N \exp(\frac{s_{kj}}{\tau})}\right], \quad (13)$$

where \mathcal{A} is the set of activated rare prototype indices for the input, s_{kj} denotes the similarity between the input representation and the j -th rare prototype. $\mathcal{L}_{\text{rare}}$ pulls the input representation closer to the activated rare prototype in the latent space while pushing it away from other rare prototypes.

Furthermore, we adopt a diversity loss \mathcal{L}_{div} that leverages orthogonal constraints to promote diversity and reduce redundancy among common prototypes, thereby ensuring the common bank covers a more comprehensive range of prevalent patterns:

$$\mathcal{L}_{\text{div}} = \frac{1}{M(M-1)} \sum_{i=1}^M \sum_{j \neq i}^M \left(\frac{\mathbf{p}_c^i \top \mathbf{p}_c^j}{\|\mathbf{p}_c^i\| \|\mathbf{p}_c^j\|} \right)^2, \quad (14)$$

where M is the number of common prototypes and \mathbf{p}_c^i is the i -th common prototype vector.

Finally, we integrated this three loss terms as the Disentanglement-Guided Loss \mathcal{L}_{DGL} :

$$\mathcal{L}_{\text{DGL}} = \lambda_{\text{sep}} \mathcal{L}_{\text{sep}} + \lambda_{\text{rare}} \mathcal{L}_{\text{rare}} + \lambda_{\text{div}} \mathcal{L}_{\text{div}}, \quad (15)$$

where $\lambda_{\text{sep}}, \lambda_{\text{rare}}, \lambda_{\text{div}}$ are balancing coefficients. The total loss function is formulated as follows:

$$\mathcal{L} = \mathcal{L}_{\text{MSE}} + \mathcal{L}_{\text{DGL}} \quad (16)$$

By explicitly coordinating the separation, preservation, and diversity of temporal prototypes, our DGLoss shapes a well-structured and disentangled pattern memory. This mechanism enables the model to dynamically retrieve context-aware patterns, effectively mitigating the limitation of static representation.

4 Experiments

To comprehensively verify the performance and effectiveness of the proposed DPAD, we conduct extensive experiments on both long-term and short-term forecasting tasks.

4.1 Experimental Setup

4.1.1 Datasets. We conduct long-term forecasting experiments on 6 real-world datasets, including (1) ETT (ETTh1, ETTh2, ETTm1, ETTm2) contains 7 features of electricity transformer data from July 2016 to July 2018, which was sampled at hourly (ETTh1, ETTh2) and 15-minute (ETTM1, ETTM2) intervals. (2) Electricity (ECL) records hourly electricity consumption data of 321 clients from 2012 to 2014. (3) Exchange collects the daily exchange-rate data from eight different countries. (4) Solar-Energy contains the solar power production of 137 PV plants in 2006, which is sampled every 10 minutes. (5) Weather includes 21 meteorological factors collected every 10 minutes from the Max Planck Biogeochemistry Institute’s Weather Station in 2020. (6) Traffic contains hourly road occupancy rates from 862 sensors on San Francisco freeways. Meanwhile, we conduct short-term forecasting experiments on PEMS (PEMS03, PEMS04, PEMS07, PEMS08), which contains the public traffic network data in California with a 5-minute interval. The details of datasets are listed in Table 1.

4.1.2 Baselines. To verify the performance and effectiveness of our DPAD, we select five state-of-the-art (SOTA) time series forecasting models with diverse architectures, including transformer-based models: iTransformer [18], TimeXer [40], TimeBridge [17]; MLP-based models: DLinear [49]; and CNN-based models: TimesNet [43].

4.1.3 Implementation Details. All experiments are implemented in PyTorch, and conducted on a single NVIDIA RTX 4090 24 GB GPU. We utilize ADAM optimizer with an initial learning rate 10^{-3} and L2 loss for model optimization. For fair evaluation, we use the framework of TimesNet [43], and all the baselines are implemented based on the configurations of original paper and its code.

Table 1. Dataset Descriptions. Num is the number of variable. Dataset size is organized in (Train, Validation, Test).

Name	Domain	Length	Num	Prediction Length	Dataset Size	Freq. (m)
ETTh1	Temperature	14400	7	{96,192,336,720}	(8545,2881,2881)	60
ETTh2	Temperature	14400	7	{96,192,336,720}	(8545,2881,2881)	60
ETTh1	Temperature	57600	7	{96,192,336,720}	(34465,11521,11521)	15
ETTh2	Temperature	57600	7	{96,192,336,720}	(34465,11521,11521)	15
Electricity	Electricity	26304	321	{96,192,336,720}	(18317,2633,5261)	60
Exchange	Exchange Rate	7588	8	{96,192,336,720}	(5120,665,1422)	1440
Traffic	Road Occupancy	17544	862	{96,192,336,720}	(12185,1757,3509)	60
Weather	Weather	52696	21	{96,192,336,720}	(36792,5271,10540)	10
Solar-Energy	Energy	52179	137	{96,192,336,720}	(36601,5161,10417)	10
PEMS03	Traffic Flow	26208	358	{12,24,48,96}	(15617,5135,5135)	5
PEMS04	Traffic Flow	16992	307	{12,24,48,96}	(10172,3375,3375)	5
PEMS07	Traffic Flow	28224	883	{12,24,48,96}	(16711,5622,5622)	5
PEMS08	Traffic Flow	17856	170	{12,24,48,96}	(10690,3548,3548)	5

4.1.4 *Metrics Details.* To evaluate forecasting performance for TSF, we utilize the mean square error (MSE) and mean absolute error (MAE). The calculations of metrics are as follows:

$$\text{MSE} = \frac{1}{n} \sum_{i=1}^n (Y_i - \hat{Y}_i)^2, \quad \text{MAE} = \frac{1}{n} \sum_{i=1}^n |Y_i - \hat{Y}_i|. \quad (17)$$

4.2 Main Results

We present the main results for both long-term and short-term forecasting on seven real-world datasets for five state-of-art forecasting models in Table 2 and Table 3, where the lower MSE and MAE indicate better forecasting performance. Our proposed DPAD framework demonstrates consistent improvements across all backbone models, achieving the lowest MSE and MAE in most cases. Notably, DPAD achieves an average MSE reduction of 12.6% for DLinear and 9.3% for iTransformer, and follows a similar trend for other backbones. The performance gains are particularly substantial on datasets with inherent complexities such as Traffic and PEMS. This reduction demonstrates the effectiveness of our model-agnostic design, which equips diverse architectures with context-aware and pattern disentanglement capability without modifying their core structure. The above observations highlight the efficacy of DPAD in mitigating the inherent limitations of static representation in forecasting models.

4.3 Ablation Studies

To validate the contribution of each component in our DPAD framework, systematic ablation experiments were conducted on Electricity, Weather, Traffic and Solar datasets. The results are presented in Table 4.

For the Dynamic Dual-Prototype bank (DDP) components, we performed the following experiments: ① without the complete DDP, ② with only the Common Bank, ③ with only the Rare Bank. As shown in Table 4, removing the entire DDP significantly degrades performance, confirming its overall effectiveness. Interestingly, using either bank alone yields marginal or even negative gains compared to the baseline, while combining both achieves the best performance.

Table 2. Forecasting results of long-term forecasting. All the results are selected from 4 different prediction lengths {96, 192, 336, 720}, and the look-back length is fixed to 96 for all baselines. The better results are highlighted in **bold**.

Methods	iTransformer				DLinear				TimesNet				TimeXer				TimeBridge				
	Ori		+DPAD		Ori		+DPAD		Ori		+DPAD		Ori		+DPAD		Ori		+DPAD		
Metric	MSE	MAE	MSE	MAE	MSE	MAE	MSE	MAE	MSE	MAE	MSE	MAE	MSE	MAE	MSE	MAE	MSE	MAE	MSE	MAE	
ETTm1	96	0.387	0.405	0.383	0.401	0.397	0.412	0.388	0.403	0.415	0.429	0.419	0.423	0.386	0.404	0.379	0.398	0.377	0.395	0.371	0.388
	192	0.441	0.436	0.433	0.423	0.446	0.441	0.431	0.432	0.479	0.466	0.471	0.460	0.429	0.435	0.433	0.430	0.427	0.425	0.423	0.421
	336	0.494	0.463	0.478	0.452	0.489	0.467	0.478	0.459	0.517	0.482	0.504	0.473	0.484	0.457	0.472	0.446	0.477	0.456	0.461	0.441
	720	0.488	0.483	0.492	0.482	0.513	0.511	0.501	0.506	0.505	0.490	0.512	0.496	0.544	0.513	0.483	0.493	0.521	0.498	0.473	0.474
	Avg	0.452	0.446	0.446	0.439	0.461	0.457	0.449	0.450	0.479	0.466	0.476	0.463	0.460	0.452	0.442	0.441	0.450	0.443	0.432	0.431
ETTm2	96	0.301	0.350	0.293	0.345	0.341	0.394	0.332	0.381	0.316	0.358	0.309	0.358	0.284	0.337	0.276	0.331	0.294	0.345	0.287	0.333
	192	0.380	0.399	0.374	0.393	0.482	0.479	0.466	0.471	0.415	0.414	0.397	0.407	0.366	0.391	0.366	0.392	0.377	0.395	0.359	0.380
	336	0.423	0.431	0.416	0.425	0.591	0.541	0.535	0.512	0.452	0.448	0.433	0.436	0.438	0.438	0.424	0.429	0.424	0.433	0.408	0.418
	720	0.431	0.447	0.422	0.435	0.839	0.661	0.785	0.638	0.461	0.463	0.448	0.455	0.407	0.449	0.411	0.432	0.423	0.442	0.417	0.435
	Avg	0.383	0.406	0.376	0.399	0.563	0.518	0.529	0.500	0.411	0.420	0.396	0.414	0.373	0.403	0.369	0.396	0.379	0.403	0.367	0.391
ETTm1	96	0.341	0.376	0.332	0.369	0.346	0.374	0.334	0.369	0.336	0.375	0.329	0.371	0.318	0.356	0.320	0.358	0.324	0.362	0.311	0.345
	192	0.382	0.396	0.377	0.389	0.382	0.391	0.375	0.392	0.377	0.395	0.376	0.393	0.373	0.389	0.366	0.383	0.365	0.384	0.361	0.375
	336	0.420	0.421	0.411	0.412	0.415	0.415	0.405	0.415	0.418	0.420	0.405	0.409	0.412	0.387	0.407	0.394	0.398	0.407	0.392	0.397
	720	0.487	0.456	0.484	0.451	0.473	0.451	0.465	0.443	0.541	0.481	0.493	0.464	0.460	0.450	0.451	0.441	0.462	0.444	0.455	0.431
	Avg	0.407	0.412	0.401	0.405	0.404	0.407	0.394	0.404	0.418	0.417	0.400	0.409	0.390	0.395	0.386	0.394	0.387	0.399	0.379	0.387
ETTm2	96	0.186	0.272	0.179	0.263	0.193	0.293	0.190	0.295	0.188	0.268	0.181	0.264	0.172	0.254	0.165	0.251	0.177	0.260	0.176	0.254
	192	0.252	0.312	0.245	0.306	0.284	0.361	0.273	0.353	0.250	0.306	0.243	0.304	0.241	0.302	0.238	0.300	0.243	0.303	0.242	0.298
	336	0.315	0.351	0.309	0.344	0.382	0.429	0.367	0.415	0.306	0.341	0.298	0.337	0.301	0.340	0.397	0.331	0.303	0.342	0.304	0.338
	720	0.415	0.408	0.409	0.405	0.558	0.525	0.508	0.501	0.420	0.405	0.402	0.398	0.394	0.395	0.396	0.393	0.401	0.399	0.409	0.397
	Avg	0.292	0.335	0.285	0.329	0.354	0.402	0.334	0.391	0.291	0.330	0.281	0.325	0.277	0.322	0.299	0.318	0.281	0.326	0.282	0.321
Electricity	96	0.148	0.241	0.147	0.234	0.211	0.302	0.202	0.293	0.163	0.267	0.159	0.269	0.241	0.244	0.141	0.241	0.143	0.239	0.135	0.228
	192	0.167	0.248	0.162	0.251	0.211	0.305	0.203	0.293	0.184	0.284	0.178	0.281	0.159	0.260	0.153	0.257	0.161	0.256	0.154	0.247
	336	0.179	0.271	0.172	0.271	0.223	0.319	0.210	0.304	0.196	0.297	0.205	0.303	0.177	0.276	0.177	0.271	0.176	0.272	0.172	0.264
	720	0.208	0.298	0.201	0.289	0.258	0.351	0.243	0.332	0.232	0.325	0.243	0.331	0.229	0.321	0.210	0.306	0.204	0.297	0.201	0.288
	Avg	0.175	0.264	0.170	0.261	0.225	0.319	0.214	0.305	0.193	0.293	0.196	0.296	0.201	0.275	0.170	0.268	0.171	0.266	0.165	0.256
Exchange	96	0.088	0.208	0.081	0.202	0.098	0.233	0.095	0.228	0.115	0.242	0.097	0.224	0.094	0.214	0.086	0.205	0.113	0.236	0.084	0.201
	192	0.180	0.303	0.175	0.299	0.186	0.325	0.182	0.319	0.216	0.333	0.186	0.310	0.182	0.303	0.179	0.301	0.200	0.327	0.177	0.297
	336	0.331	0.418	0.326	0.414	0.325	0.434	0.329	0.442	0.375	0.444	0.360	0.434	0.384	0.448	0.350	0.426	0.364	0.440	0.339	0.421
	720	0.848	0.695	0.835	0.692	0.746	0.663	0.772	0.678	0.101	0.765	0.893	0.720	0.932	0.724	0.887	0.706	0.992	0.760	0.847	0.691
	Avg	0.361	0.406	0.354	0.401	0.338	0.413	0.345	0.417	0.201	0.446	0.384	0.422	0.398	0.422	0.375	0.409	0.417	0.440	0.361	0.402
Solar	96	0.207	0.237	0.199	0.221	0.290	0.378	0.240	0.299	0.223	0.256	0.211	0.249	0.198	0.244	0.191	0.235	0.204	0.245	0.196	0.212
	192	0.242	0.264	0.237	0.254	0.320	0.398	0.263	0.312	0.262	0.272	0.241	0.267	0.226	0.270	0.221	0.262	0.237	0.269	0.228	0.236
	336	0.251	0.277	0.249	0.273	0.353	0.415	0.279	0.314	0.287	0.299	0.257	0.291	0.239	0.281	0.231	0.275	0.251	0.283	0.247	0.256
	720	0.251	0.278	0.250	0.276	0.357	0.413	0.276	0.310	0.298	0.318	0.267	0.298	0.242	0.282	0.238	0.277	0.253	0.284	0.255	0.260
	Avg	0.237	0.264	0.233	0.256	0.330	0.401	0.264	0.308	0.267	0.286	0.244	0.276	0.226	0.269	0.220	0.262	0.236	0.270	0.231	0.241
Traffic	96	0.393	0.269	0.392	0.268	0.712	0.438	0.647	0.402	0.593	0.317	0.471	0.295	0.428	0.271	0.415	0.263	0.375	0.270	0.371	0.243
	192	0.412	0.277	0.407	0.271	0.662	0.417	0.599	0.380	0.618	0.327	0.493	0.309	0.447	0.280	0.442	0.273	1.411	0.803	0.397	0.254
	336	0.424	0.283	0.417	0.279	0.669	0.419	0.590	0.374	0.642	0.341	0.514	0.320	0.472	0.289	0.473	0.290	1.427	0.806	0.408	0.261
	720	0.459	0.301	0.447	0.293	0.709	0.437	0.616	0.385	0.679	0.350	0.568	0.351	0.517	0.307	0.522	0.310	0.435	0.298	0.602	0.387
	Avg	0.422	0.282	0.416	0.278	0.688	0.427	0.613	0.385	0.633	0.333	0.511	0.318	0.466	0.286	0.463	0.284	0.912	0.544	0.444	0.286
Weather	96	0.176	0.216	0.170	0.208	0.195	0.252	0.187	0.255	0.172	0.221	0.156	0.204	0.157	0.205	0.151	0.201	0.177	0.218	0.173	0.210
	192	0.225	0.257	0.223	0.256	0.239	0.299	0.228	0.291	0.220	0.260	0.207	0.249	0.204	0.248	0.202	0.244	0.223	0.258	0.216	0.251
	336	0.281	0.299	0.279	0.295	0.282	0.333	0.273	0.335	0.280	0.302	0.265</									

Table 3. Forecasting results of short-term forecasting. All the results are selected from 4 different prediction lengths {12, 24, 48, 96}, and the look-back length is fixed to 96 for all baselines. The better results are highlighted in **bold**.

Methods	iTransformer				DLinear				TimesNet				TimeXer				TimeBridge				
	Ori		+DPAD		Ori		+DPAD		Ori		+DPAD		Ori		+DPAD		Ori		+DPAD		
Metric	MSE	MAE	MSE	MAE	MSE	MAE	MSE	MAE	MSE	MAE	MSE	MAE	MSE	MAE	MSE	MAE	MSE	MAE	MSE	MAE	
PEMS03	12	0.069	0.175	0.067	0.169	0.122	0.245	0.102	0.218	0.088	0.195	0.066	0.172	0.068	0.179	0.077	0.183	0.075	0.183	0.072	0.178
	24	0.099	0.210	0.102	0.213	0.202	0.320	0.141	0.257	0.118	0.224	0.091	0.198	0.089	0.204	0.091	0.211	0.105	0.219	0.102	0.212
	48	0.164	0.275	0.169	0.281	0.334	0.428	0.226	0.329	0.169	0.268	0.137	0.244	0.137	0.253	0.134	0.249	0.171	0.284	0.169	0.278
	96	0.711	0.651	0.417	0.472	0.459	0.517	0.319	0.403	0.239	0.330	0.206	0.303	0.427	0.483	0.236	0.349	0.262	0.365	0.267	0.370
	Avg	0.260	0.327	0.188	0.283	0.279	0.377	0.197	0.301	0.153	0.254	0.125	0.229	0.180	0.279	0.134	0.248	0.153	0.262	0.155	0.259
PEMS04	12	0.766	0.709	0.115	0.241	0.147	0.272	0.114	0.233	0.092	0.202	0.073	0.179	0.293	0.397	0.083	0.198	0.097	0.206	0.093	0.198
	24	0.799	0.728	0.157	0.280	0.225	0.340	0.157	0.275	0.111	0.224	0.088	0.198	0.308	0.409	0.105	0.229	0.133	0.243	0.134	0.240
	48	1.041	0.882	0.229	0.341	0.356	0.437	0.239	0.343	0.152	0.266	0.118	0.234	0.339	0.425	0.146	0.272	0.215	0.319	0.216	0.313
	96	1.045	0.886	0.293	0.388	0.453	0.505	0.312	0.401	0.197	0.308	0.167	0.279	0.367	0.441	0.219	0.343	0.329	0.412	0.324	0.407
	Avg	0.912	0.801	0.199	0.312	0.295	0.388	0.205	0.313	0.138	0.250	0.111	0.222	0.326	0.418	0.138	0.261	0.193	0.295	0.192	0.289
PEMS07	12	0.068	0.169	0.065	0.161	0.116	0.241	0.100	0.210	0.075	0.179	0.063	0.162	0.061	0.165	0.056	0.161	0.067	0.168	0.066	0.163
	24	0.087	0.190	0.081	0.187	0.209	0.327	0.149	0.261	0.083	0.198	0.080	0.183	0.071	0.177	0.067	0.171	0.095	0.200	0.096	0.196
	48	0.122	0.231	0.118	0.225	0.397	0.456	0.269	0.347	0.128	0.235	0.118	0.221	0.100	0.208	0.109	0.211	0.145	0.252	0.148	0.248
	96	0.159	0.267	0.152	0.258	0.592	0.552	0.374	0.422	0.150	0.253	0.162	0.261	0.120	0.221	0.124	0.225	0.206	0.310	0.211	0.312
	Avg	0.109	0.214	0.104	0.207	0.328	0.394	0.223	0.310	0.109	0.216	0.105	0.206	0.088	0.192	0.089	0.192	0.128	0.232	0.130	0.230
PEMS08	12	0.081	0.183	0.078	0.179	0.153	0.259	0.148	0.234	0.158	0.192	0.082	0.185	0.146	0.198	0.088	0.204	0.080	0.184	0.075	0.178
	24	0.118	0.222	0.113	0.219	0.238	0.357	0.192	0.277	0.112	0.219	0.108	0.212	0.171	0.221	0.125	0.241	0.112	0.217	0.110	0.213
	48	0.202	0.292	0.210	0.294	0.473	0.515	0.310	0.353	0.231	0.198	0.166	0.221	0.220	0.270	0.208	0.283	0.186	0.278	0.181	0.272
	96	0.395	0.415	0.294	0.326	0.748	0.646	0.441	0.429	0.291	0.338	0.287	0.324	0.285	0.303	0.296	0.321	0.296	0.344	0.292	0.340
	Avg	0.199	0.278	0.173	0.254	0.403	0.444	0.272	0.323	0.198	0.236	0.160	0.235	0.205	0.248	0.179	0.262	0.168	0.255	0.164	0.251

Table 4. Results of ablation study. All the results are selected from 4 different prediction lengths {96, 192, 336, 720}, and the look-back length is fixed to 96 for all baselines. The better results are highlighted in **bold**.

Case	+DPAD		Ⓔw/o DDP		Ⓔw/o Common		Ⓔw/o Rare		Ⓔw/o Additive		Ⓔw/o Mean		Ⓔw/o \mathcal{L}_{DGL}		Ⓔw/o \mathcal{L}_{sep}		Ⓔw/o \mathcal{L}_{rare}		Ⓔw/o \mathcal{L}_{div}		
Metric	MSE	MAE	MSE	MAE	MSE	MAE	MSE	MAE	MSE	MAE	MSE	MAE	MSE	MAE	MSE	MAE	MSE	MAE	MSE	MAE	
Electricity	96	0.147	0.234	0.148	0.241	0.152	0.243	0.155	0.244	0.153	0.242	0.149	0.245	0.151	0.240	0.154	0.242	0.154	0.239	0.151	0.240
	192	0.162	0.251	0.167	0.248	0.167	0.259	0.170	0.261	0.169	0.260	0.167	0.263	0.171	0.264	0.168	0.262	0.166	0.259	0.165	0.260
	336	0.172	0.271	0.179	0.271	0.178	0.271	0.181	0.273	0.182	0.272	0.181	0.275	0.183	0.275	0.180	0.273	0.182	0.275	0.184	0.277
	720	0.201	0.192	0.208	0.298	0.216	0.303	0.225	0.310	0.213	0.298	0.212	0.294	0.217	0.305	0.209	0.301	0.212	0.297	0.208	0.299
	Avg	0.170	0.237	0.175	0.264	0.178	0.269	0.183	0.272	0.179	0.268	0.177	0.269	0.181	0.271	0.178	0.269	0.179	0.268	0.177	0.269
Weather	96	0.17	0.208	0.176	0.216	0.175	0.214	0.175	0.215	0.178	0.216	0.173	0.212	0.177	0.216	0.173	0.212	0.175	0.216	0.172	0.212
	192	0.223	0.256	0.225	0.257	0.229	0.261	0.230	0.262	0.228	0.259	0.227	0.260	0.231	0.263	0.229	0.260	0.229	0.259	0.230	0.261
	336	0.279	0.295	0.281	0.299	0.283	0.300	0.285	0.302	0.283	0.299	0.282	0.301	0.286	0.302	0.284	0.300	0.283	0.303	0.282	0.301
	720	0.355	0.347	0.361	0.353	0.362	0.353	0.361	0.351	0.361	0.352	0.359	0.352	0.363	0.352	0.360	0.352	0.359	0.352	0.358	0.352
	Avg	0.256	0.276	0.260	0.281	0.262	0.282	0.263	0.282	0.262	0.282	0.260	0.281	0.264	0.283	0.262	0.281	0.262	0.283	0.261	0.282
Traffic	96	0.392	0.268	0.393	0.269	0.477	0.337	0.395	0.272	0.396	0.270	0.459	0.325	0.457	0.323	0.426	0.314	0.433	0.310	0.468	0.333
	192	0.407	0.271	0.412	0.277	0.414	0.277	0.413	0.277	0.412	0.276	0.413	0.279	0.418	0.282	0.478	0.333	0.415	0.280	0.412	0.277
	336	0.417	0.279	0.424	0.283	0.425	0.283	0.427	0.284	0.425	0.284	0.425	0.286	0.429	0.286	0.424	0.282	0.493	0.340	0.425	0.282
	720	0.447	0.293	0.459	0.301	0.531	0.359	0.457	0.300	0.454	0.299	0.457	0.301	0.459	0.302	0.459	0.302	0.461	0.301	0.458	0.303
	Avg	0.416	0.278	0.422	0.282	0.462	0.314	0.423	0.283	0.422	0.282	0.439	0.298	0.441	0.298	0.464	0.322	0.450	0.308	0.441	0.299
Solar	96	0.199	0.221	0.207	0.237	0.206	0.239	0.204	0.233	0.205	0.247	0.203	0.236	0.210	0.241	0.208	0.241	0.209	0.240	0.206	0.243
	192	0.237	0.254	0.242	0.264	0.244	0.268	0.240	0.260	0.239	0.267	0.239	0.261	0.240	0.266	0.239	0.265	0.240	0.266	0.241	0.259
	336	0.249	0.273	0.251	0.277	0.254	0.278	0.252	0.275	0.253	0.278	0.250	0.275	0.255	0.281	0.254	0.280	0.255	0.279	0.253	0.280
	720	0.250	0.276	0.251	0.278	0.256	0.280	0.252	0.278	0.253	0.279	0.254	0.277	0.260	0.282	0.254	0.279	0.254	0.280	0.253	0.279
	Avg	0.233	0.256	0.237	0.262	0.240	0.266	0.237	0.262	0.237	0.268	0.237	0.262	0.241	0.267	0.239	0.266	0.239	0.266	0.238	0.265

functionality of our DPC mechanism, which dynamically adjusts the contribution of retrieved prototypes according to specific input contexts.

For the Disentanglement-Guided Loss (DGLoss), we conduct experiments as follows: Ⓔ removes all components in DGLoss, Ⓕ removes the separation loss \mathcal{L}_{sep} , Ⓖ removes the rarity preservation loss \mathcal{L}_{rare} , and Ⓗ removes the diversity loss \mathcal{L}_{div} . As shown in Table 4, removing any individual loss term or the whole DGLoss leads to a performance drop. Training without these specialized constraints fails to effectively optimize the interaction between the model and our prototype banks. Meanwhile, without explicit guidance for separation, diversity, and rarity preservation, our DDP

Table 5. Zero-shot forecasting results on ETT datasets. The forecasting length is set to 96. And the better results are highlighted in **bold**.

Methods		iTransformer		+DPAD		DLinear		+DPAD		TimesNet		+DPAD		TimeXer		+DPAD	
Source	Target	MSE	MAE	MSE	MAE	MSE	MAE	MSE	MAE	MSE	MAE	MSE	MAE	MSE	MAE	MSE	MAE
ETTh1	ETTh2	0.419	0.428	0.416	0.425	0.495	0.487	0.489	0.481	0.480	0.459	0.439	0.443	0.426	0.429	0.420	0.425
	ETTh1	0.822	0.585	0.834	0.596	0.749	0.579	0.746	0.576	0.849	0.575	0.754	0.571	0.832	0.591	0.798	0.575
	ETTh2	0.342	0.375	0.339	0.373	0.409	0.454	0.405	0.451	0.368	0.390	0.339	0.370	0.344	0.374	0.341	0.370
ETTh2	ETTh1	0.694	0.581	0.632	0.547	0.544	0.508	0.539	0.504	0.802	0.623	0.769	0.602	0.695	0.577	0.666	0.558
	ETTh2	0.980	0.631	0.904	0.606	0.768	0.594	0.783	0.605	1.059	0.658	1.043	0.644	1.428	0.748	1.412	0.734
	ETTh1	0.358	0.389	0.346	0.378	0.537	0.541	0.526	0.532	0.369	0.394	0.380	0.404	0.387	0.408	0.377	0.402
ETTh1	ETTh2	0.718	0.571	0.670	0.549	0.614	0.530	0.602	0.522	0.952	0.694	0.930	0.660	0.960	0.662	0.948	0.643
	ETTh1	0.482	0.465	0.476	0.459	0.500	0.492	0.492	0.479	0.566	0.515	0.555	0.507	0.591	0.522	0.578	0.507
	ETTh2	0.326	0.362	0.312	0.351	0.318	0.356	0.337	0.367	0.357	0.380	0.340	0.369	0.336	0.364	0.341	0.371
ETTh2	ETTh1	1.214	0.748	0.980	0.676	0.634	0.554	0.611	0.523	0.993	0.655	0.872	0.619	0.734	0.578	0.709	0.576
	ETTh2	0.553	0.507	0.519	0.487	0.508	0.499	0.519	0.506	0.528	0.487	0.490	0.472	0.457	0.453	0.436	0.425
	ETTh1	0.825	0.589	0.804	0.579	0.561	0.498	0.544	0.479	0.709	0.554	0.701	0.548	0.647	0.531	0.631	0.525

cannot learn a well-disentangled representation, and their synergistic effect will be severely compromised. Therefore, DGLoss serves as a core component that ensures effective pattern disentanglement and stable prototype memory formation.

4.4 Zero-Shot Forecasting

To further evaluate the generalization and robustness of our DPAD on unseen datasets, we conduct zero-shot forecasting experiments. Following prior works [13, 15], we sequentially use ETTh1, ETTh2, ETTh1, and ETTh2 as source datasets, and the remaining datasets as target datasets.

Table 5 shows zero-shot results with four backbone models, which consistently demonstrate that models enhanced with our DPAD framework achieve superior performance in most cases. These improvements indicate that the disentangled pattern memory in DPAD provides a more transferable and robust temporal representation. Specifically, the common prototypes in DDP learn domain-invariant, prevalent patterns that serve as reusable components across different datasets. Meanwhile, the DPC mechanism enables the model to dynamically integrate these prototypes, and activate sparse rare prototypes when necessary, which could account for novel, target-specific variations without requiring retraining. Consequently, these zero-shot results underscore that DPAD not only enhances forecasting performance for in-distribution data, but also learns temporal patterns with more generalization.

4.5 Comparison Results with other Enhancement Strategies

To further validate the effectiveness of DPAD, we compare it against several representative model-agnostic enhancement strategies that adopt different technical paradigms. RAFT [9] employs retrieval augmented generation to enhance forecasting by querying historical samples. HCAN[32] proposes a hierarchy-aware attention module supported by uncertainty-aware classifiers and a consistency loss to alleviate issues caused by the boundary effects during the classification of timesteps. FreDF [35] bypasses the complexity of label autocorrelation by learning to forecast in the frequency domain. As shown in Table 6, DPAD consistently achieves superior performance in most cases across various datasets and forecasting horizons. This is due to its unified framework for context-aware and pattern disentanglement, which addresses the core limitations of static representation more directly than other strategies. Thus DPAD demonstrates consistently strong generalization across diverse forecasting scenarios.

Table 6. Forecasting results compared with other enhancement strategies on Electricity, ETTh2, and Weather datasets. We use iTransformer as backbone for HCAN, FreDF, and DPAD. The best results are highlighted in **bold**, and the second-best results are highlighted in underline.

Dataset		Electricity				ETTh2				Weather			
Forecast length		96	192	336	720	96	192	336	720	96	192	336	720
ori (2024a)	MSE	<u>0.148</u>	0.167	<u>0.179</u>	<u>0.208</u>	0.301	0.380	0.423	0.431	0.176	0.225	0.281	0.361
	MAE	<u>0.241</u>	0.248	<u>0.271</u>	<u>0.298</u>	0.350	0.399	0.431	0.447	0.216	0.257	0.299	0.353
RAFT (2025)	MSE	0.168	0.172	0.182	0.212	0.288	0.384	0.432	0.436	0.190	0.241	0.294	0.370
	MAE	0.269	0.270	0.281	0.304	0.341	0.402	0.443	0.460	0.237	0.281	0.323	0.374
HCAN (2024)	MSE	0.588	0.484	0.466	0.440	0.776	1.208	1.123	1.857	0.219	0.274	0.307	0.353
	MAE	0.603	0.530	0.516	0.499	0.656	0.813	0.787	1.119	0.301	0.348	0.371	0.400
FreDF (2025b)	MSE	0.158	<u>0.166</u>	0.188	0.225	<u>0.290</u>	0.373	<u>0.418</u>	<u>0.426</u>	<u>0.171</u>	<u>0.224</u>	<u>0.282</u>	0.359
	MAE	0.248	0.259	0.277	0.308	<u>0.342</u>	<u>0.394</u>	<u>0.429</u>	<u>0.443</u>	<u>0.209</u>	0.255	<u>0.298</u>	<u>0.350</u>
+ DPAD	MSE	0.147	0.162	0.172	0.201	0.293	<u>0.374</u>	0.416	0.422	0.170	0.223	0.279	<u>0.355</u>
	MAE	0.234	<u>0.251</u>	0.271	0.289	0.345	0.393	0.425	0.435	0.208	<u>0.256</u>	0.295	0.347

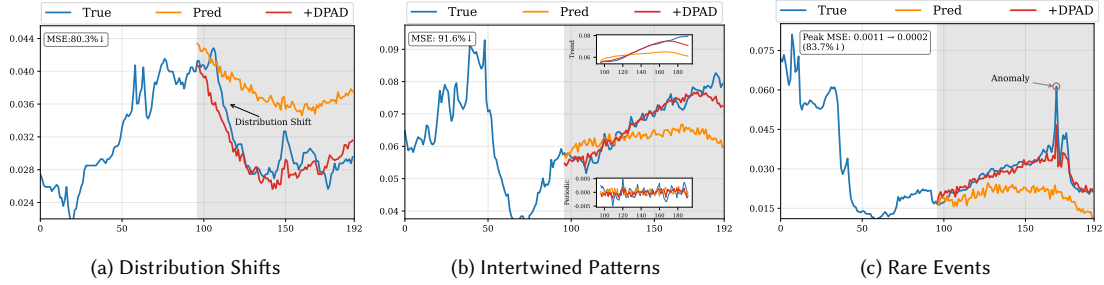


Fig. 3. Case studies on failure scenarios: a) distribution shifts; b) intertwined patterns; c) rare events.

4.6 Case Studies On Failure Scenarios

To directly verify that DPAD mitigates the three failure cases introduced in Section 1, we select representative sequences from the Weather datasets. As shown in Figure 3, for (a) distribution shifts, the backbone fails to fully adapt to changes in data distribution after a temporal shift, while the common bank in DPAD provides stable reference prototypes that persist across this cases, enabling the model to maintain more reliable predictions. For (b) intertwined patterns, where a linear trend coexists with multi-frequency periodic components, the backbone inadequately captures these patterns, whereas DPAD selectively retrieves relevant prototypes via its dual-path routing mechanism, thus effectively disentangling the intertwined patterns. For (c) rare events, characterized by a sudden temperature spike, the backbone yields a large peak error, while DPAD reduces the MSE in the peak region by 83.7%. This improvements is attributed to the rare bank and rarity preservation loss, which preserve infrequent events without enforcing overfitting. Collectively, these case studies demonstrate that the three components in DPAD jointly address the core limitations of static representation learning in time series forecasting.

4.7 Model Analysis

4.7.1 Prototype Visualization. To provide an intuitive understanding of what the DDP learns, we visualize the temporal forms of several representative prototypes from both the common and rare bank on the Weather dataset. As shown in

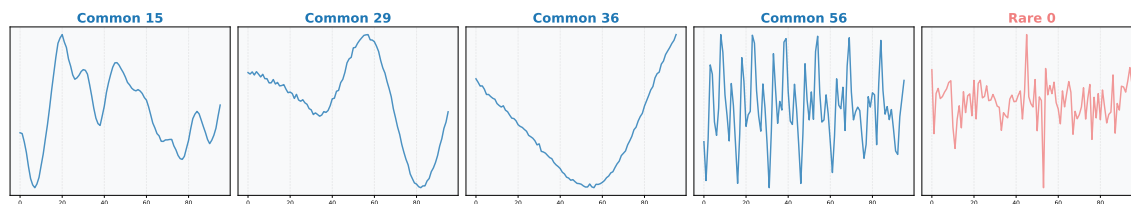


Fig. 4. Visualization of learned prototypes in DDP on the Electricity dataset.

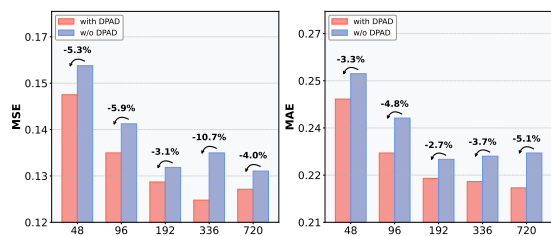


Fig. 5. Forecasting results (MSE and MAE) with varying look-back length {48, 96, 192, 336, 720} on Electricity dataset. Prediction length is fixed to 96.

Table 7. Comparison of efficiency analysis for backbone models with and without DPAD. The results are recorded on the Electricity dataset with batch size is set to 16. The look-back length and prediction length is fixed to 96. Running time means running time per iteration. $\Delta\%$ denotes the relative change rate.

Metrics	Running Time			Memory Footprint		
	ori	+DPAD	$\Delta\%$	ori	+DPAD	$\Delta\%$
iTransformer	17ms	20ms	17.6%	782MB	820MB	4.8%
TimeXer	119ms	126ms	5.8%	4634MB	4746MB	2.4%
TimeBridge	98ms	107ms	9.1%	4240MB	4334MB	2.2%
DLinear	7ms	11ms	57.1%	62MB	90MB	45.1%
TimesNet	262ms	266ms	1.5%	3332MB	3470MB	4.1%

Figure 4, the prototypes in both the common bank and rare bank evolve dynamically during training. For the common bank, the learned prototypes consistently exhibit smooth, structured shapes, including stable hybrid patterns that combine trend and seasonality components. These patterns correspond well to the intricate dependencies of the dataset, confirming that our initialization provides effective guidance and that the common bank successfully captures and refines these prevalent patterns through training. In contrast, the rare bank displays markedly different characteristics, whose prototypes are characterized by abrupt, irregular fluctuations or sudden shifts. These patterns do not conform to regular seasonal or trend patterns, which demonstrates the capability of rare set to memorize infrequent yet critical events as well as some other fluctuations.

4.7.2 Increasing Look-Back Length. A longer look-back sequence provides richer historical information in principle, yet also presents a greater challenge due to the more complex temporal dependencies it includes. To evaluate the capability of DPAD to disentangle and leverage long-range historical context, we conduct experiments under increasing look-back length {48, 96, 192, 336, 720} on the Electricity dataset, taking TimeBridge as backbone model. As shown in Figure 5, DPAD consistently achieves greater performance gains over the backbone as the sequence length increases. While vanilla backbones may suffer from information overload or struggle to focus on long-term dependencies, DPAD helps them utilize the extended history information more effectively. These results indicate that components in DPAD are particularly effective at capturing, disentangling, and selectively leveraging relevant intertwined patterns from long sequences. Our framework provides a structured mechanism to deal with the expanded context.

4.7.3 Efficiency Analysis. We conduct the efficiency analysis for the backbone model with and without DPAD. As shown in Table 7, DPAD introduces minimal overhead for most backbone models. The relative increases in running time and memory footprint are generally modest, which are below 10% for most Transformer or CNN-based backbones. While a lightweight model like DLinear shows a higher relative increase due to its extremely small base cost, the

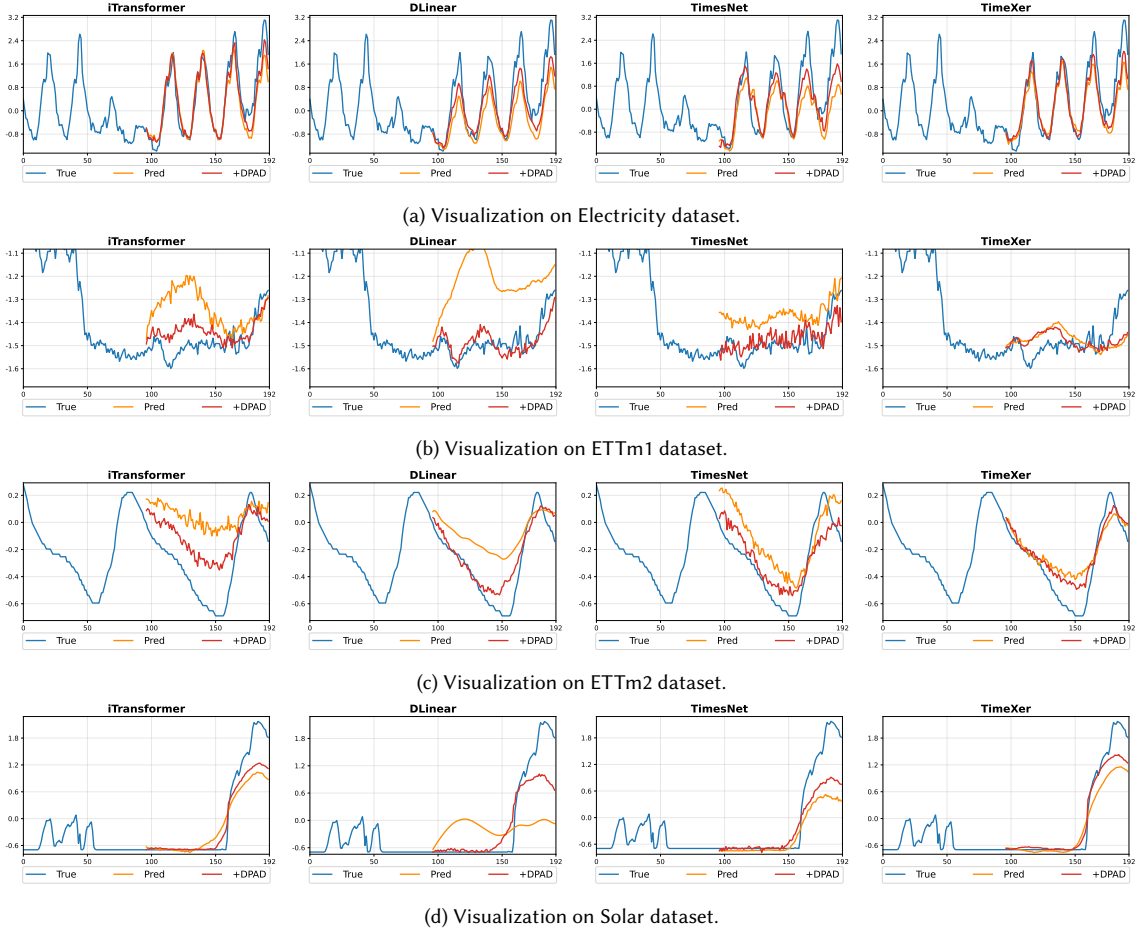


Fig. 6. Forecasting visualization for backbone models with and without DPAD.

absolute added overhead remains minimal. This demonstrates DPAD is a practical and efficient enhancement module, delivering significant performance improvements while incurring only a small fraction of additional computational cost.

4.7.4 Forecasting Visualization. To provide a more intuitive and comprehensive view of the improvements brought by our DPAD framework, we present forecasting visualizations comparing the predictions of backbone models with and without DPAD across four representative datasets. As shown in Figure 6, the predictions with DPAD are closer to the ground truth. These visualization results serve as qualitative evidence that DPAD enables more flexible, context-aware, and accurate forecasting across diverse model architectures and temporal patterns.

4.8 Hyperparameter Sensitivity Analysis

4.8.1 Size of Prototype Banks. The sizes of the Common Pattern Bank \mathcal{B}_c and Rare Pattern Bank \mathcal{B}_r determine the representational capacity and specialization degree of our Dual-Prototype Bank. To analyze their impact, we set

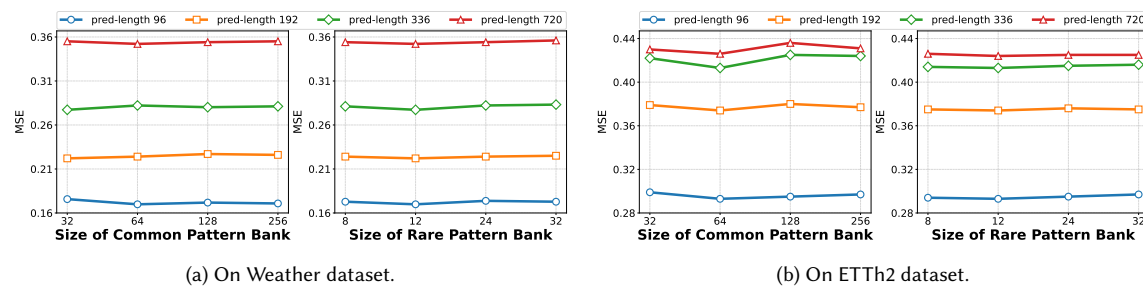


Fig. 7. Hyperparameter sensitivity analysis with varying sizes of prototype banks on Weather dataset. Here we use iTransformer as backbone. Left is of common pattern set, right is of rare patterns set. The look-back length is fixed to 96.

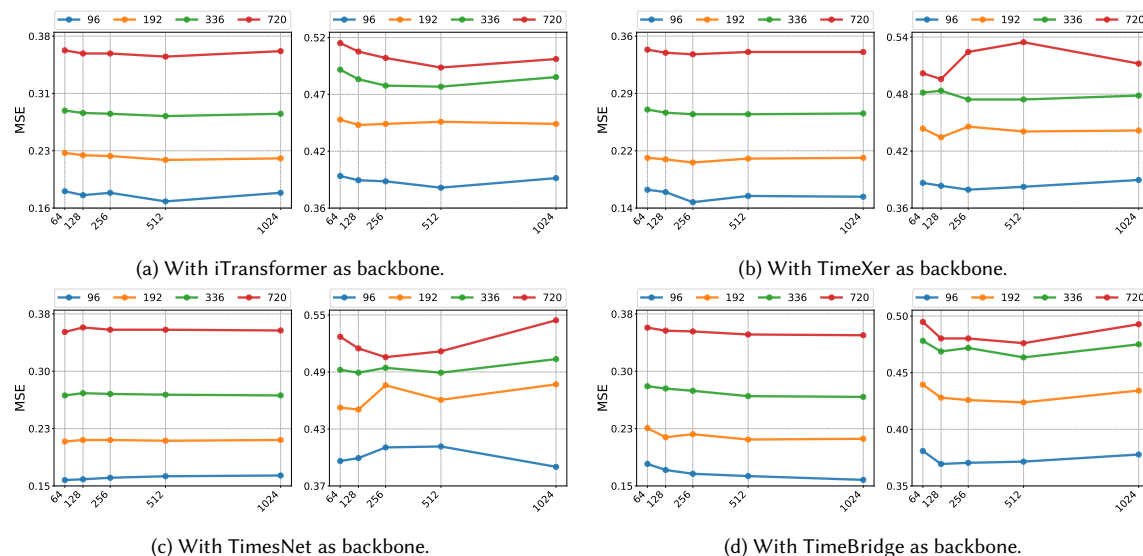


Fig. 8. Hyperparameter sensitivity analysis on embedding dimension. For each backbone, forecasting results are on the Weather (left) and ETTh1 (right) datasets. The look-back length is fixed to 96.

$\mathcal{B}_c \in \{32, 64, 128, 256\}$ and $\mathcal{B}_r \in \{8, 12, 24, 32\}$ respectively on the Weather and ETTh2 dataset. As shown in Figure 7, the results remain stable across a broad range of sizes, indicating that DPAD is not highly sensitive to the size of prototype banks. Extremely small banks may limit the ability to capture pattern diversity, while very large banks offer no further gain and may slightly degrade performance due to increased optimization difficulty. The above observation confirms that DPAD is robust across various cases without requiring delicate tuning.

4.8.2 Embedding Dimension. The embedding dimension determines the richness of feature representations in the unified projection space. We vary $d_{\text{model}} \in \{64, 128, 256, 512, 1024\}$ on the Weather and ETTh1 dataset with four backbone models to evaluate its impact. As shown in Figure 8, in most cases DPAD exhibits low sensitivity to the choice of embedding dimension. Performance does not degrade significantly even at relatively small dimensions, while larger dimensions provide only marginal gains. So we choose the optimal dimension at 128/256 in most cases. The above observation indicates that our dual-prototype architecture and routing mechanism are effective at capturing and

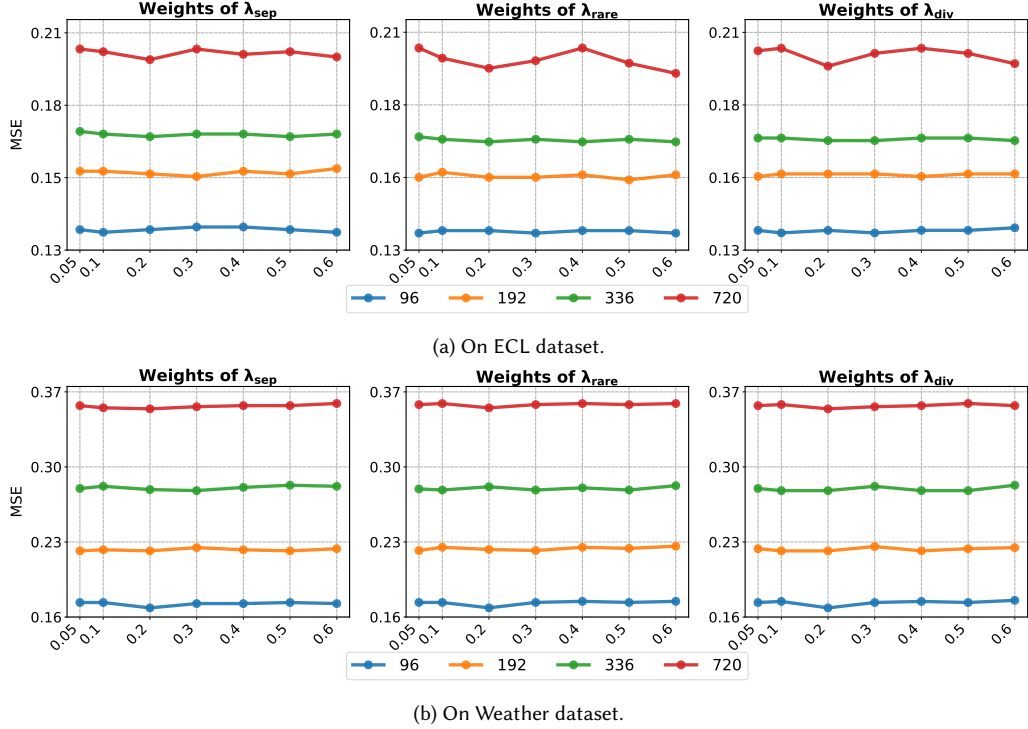


Fig. 9. Hyperparameter sensitivity analysis on weights of DGLoss. Forecasting results are on the ECL and Weather datasets, and we use TimeBridge as backbone model. The look-back length is fixed to 96.

utilizing pattern information without requiring a high-dimension latent space. This property further simplifies the deployment of DPAD as a plug-and-play module.

4.8.3 Weights of DGLoss. The weight λ_{sep} , λ_{rare} , λ_{div} of the DGLoss controls the strength of separation, rarity preservation, and diversity of temporal prototypes. To analyze their individual effects, we vary them in 0.001 – 2.0 on electricity and weather datasets. As shown in Figure 9, the forecasting performance remains stable across a wide range of weight values. Specifically, the MSE exhibit only minor fluctuations when the weights are varied from 0.001 – 2.0, indicating that the proposed DGLoss is not highly sensitive to the exact choice of these hyperparameters, which simplifies the deployment of DPAD in practice.

5 Conclusion

In this paper, we address a critical limitation of static and averaged representations in deep time series forecasting, which hinders model adaptability to intricate and dynamic contexts. We propose the Dual-Prototype Adaptive Disentanglement (DPAD) framework, a model-agnostic auxiliary method that enhances the backbone model through a Dynamic Dual-Prototype bank (DDP), Dual-Path Context-aware routing (DPC), and a Disentanglement-Guided Loss (DGLoss). Extensive experiments validate that DPAD consistently improves forecasting performance while introduces minimal computational overhead. Future work may explore more interpretable routing mechanisms and a novel prototype paradigm with multi-modal representations.

References

- [1] Francisco Martinez Alvarez, Alicia Troncoso, Jose C Riquelme, and Jesus S Aguilar Ruiz. 2010. Energy time series forecasting based on pattern sequence similarity. *IEEE Transactions on Knowledge and Data Engineering* 23, 8 (2010), 1230–1243.
- [2] Shaojie Bai, J. Zico Kolter, and Vladlen Koltun. 2018. An Empirical Evaluation of Generic Convolutional and Recurrent Networks for Sequence Modeling. *arXiv preprint arXiv:1803.01271* (2018).
- [3] Kaifeng Bi, Lingxi Xie, Hengheng Zhang, Xin Chen, and Xiaotao Gu. 2023. Accurate medium-range global weather forecasting with 3D neural networks. *Nature* 619, 7970 (2023), 533–538.
- [4] Peng Chen, Yingying Zhang, Yunyao Cheng, Yang Shu, Yihang Wang, Qingsong Wen, Bin Yang, and Chenjuan Guo. 2024. PATHFORMER: MULTI-SCALE TRANSFORMERS WITH ADAPTIVE PATHWAYS FOR TIME SERIES FORECASTING. In *12th International Conference on Learning Representations, ICLR 2024*.
- [5] Zihan Chen, Lei Zheng, Cheng Lu, Jialu Yuan, and Di Zhu. 2023. ChatGPT Informed Graph Neural Network for Stock Movement Prediction. *SSRN Electronic Journal* (2023).
- [6] Haoang Chi, Feng Liu, Wenjing Yang, Long Lan, Tongliang Liu, Bo Han, William Cheung, and James Kwok. 2021. TOHAN: A one-step approach towards few-shot hypothesis adaptation. *Advances in neural information processing systems* 34 (2021), 20970–20982.
- [7] Chenjuan Guo, Bin Yang, Ove Andersen, Christian S Jensen, and Kristian Torp. 2015. Ecomark 2.0: empowering eco-routing with vehicular environmental models and actual vehicle fuel consumption data. *Geoinformatica* 19, 3 (2015), 567–599.
- [8] Chenjuan Guo, Bin Yang, Jilin Hu, Christian S Jensen, and Lu Chen. 2020. Context-aware, preference-based vehicle routing. *The VLDB Journal* 29, 5 (2020), 1149–1170.
- [9] Sungwon Han, Seungeon Lee, Meeyoung Cha, Sercan O Arik, and Jinsung Yoon. 2025. Retrieval Augmented Time Series Forecasting. *arXiv preprint arXiv:2505.04163* (2025).
- [10] Yifan Hu, Peiyuan Liu, Peng Zhu, Dawei Cheng, and Tao Dai. 2025. Adaptive Multi-Scale Decomposition Framework for Time Series Forecasting. *arXiv preprint arXiv:2406.03751* (2025).
- [11] Songtao Huang, Zhen Zhao, Can Li, and Lei Bai. 2025. TimeKAN: KAN-based Frequency Decomposition Learning Architecture for Long-term Time Series Forecasting. *arXiv preprint arXiv:2502.06910* (2025).
- [12] KyoHoon Jin, JeongA Wi, EunJu Lee, ShinJin Kang, SookYun Kim, and YoungBin Kim. 2021. TrafficBERT: Pre-trained model with large-scale data for long-range traffic flow forecasting. *Expert Systems with Applications* 186 (2021), 115738.
- [13] Ming Jin, Shiyu Wang, Lintao Ma, Zhixuan Chu, James Y. Zhang, Xiaoming Shi, Pin-Yu Chen, Yuxuan Liang, Yuan-Fang Li, Shirui Pan, and Qingsong Wen. 2024. Time-LLM: Time Series Forecasting by Reprogramming Large Language Models. *arXiv preprint arXiv:2310.01728* (2024).
- [14] Taesung Kim, Jinhee Kim, Yunwon Tae, Cheonbok Park, Jang-Ho Choi, and Jaegul Choo. 2022. REVERSIBLE INSTANCE NORMALIZATION FOR ACCURATE TIME-SERIES FORECASTING AGAINST DISTRIBUTION SHIFT. In *10th International Conference on Learning Representations, ICLR 2022*.
- [15] Dillfira Kudrat, Zongxia Xie, Yanru Sun, Tianyu Jia, and Qinghua Hu. 2025. Patch-wise Structural Loss for Time Series Forecasting. *arXiv preprint arXiv:2503.00877* (2025).
- [16] Minhao LIU, Ailing Zeng, Muxi Chen, Zhijian Xu, Qiuxia LAI, Lingna Ma, and Qiang Xu. 2022. SCINet: Time Series Modeling and Forecasting with Sample Convolution and Interaction. In *Advances in Neural Information Processing Systems*, Vol. 35. 5816–5828.
- [17] Peiyuan Liu, Beiliang Wu, Yifan Hu, Naiqi Li, Tao Dai, Jigang Bao, and Shu tao Xia. 2025. TimeBridge: Non-Stationarity Matters for Long-term Time Series Forecasting. *arXiv preprint arXiv:2410.04442* (2025).
- [18] Yong Liu, Tengge Hu, Haoran Zhang, Haixu Wu, Shiyu Wang, Lintao Ma, and Mingsheng Long. 2024. iTransformer: Inverted Transformers Are Effective for Time Series Forecasting. *arXiv preprint arXiv:2310.06625* (2024).
- [19] Yong Liu, Haoran Zhang, Chenyu Li, Xiangdong Huang, Jianmin Wang, and Mingsheng Long. 2024. Timer: Generative Pre-trained Transformers Are Large Time Series Models. In *41st International Conference on Machine Learning, ICML 2024*.
- [20] Zhiding Liu, Mingyue Cheng, Zhi Li, Zhenya Huang, Qi Liu, Yanhu Xie, and Enhong Chen. 2023. Adaptive Normalization for Non-stationary Time Series Forecasting: A Temporal Slice Perspective. In *37th Conference on Neural Information Processing Systems, NeurIPS 2023*.
- [21] Zhiding Liu, Mingyue Cheng, Guan hao Zhao, Jiqian Yang, Qi Liu, and Enhong Chen. 2025. Improving Time Series Forecasting via Instance-aware Post-hoc Revision. *arXiv preprint arXiv:2505.23583* (2025).
- [22] Zhining Liu, Ze Yang, Xiao Lin, Ruizhong Qiu, Tianxin Wei, Yada Zhu, Hendrik Hamann, Jingrui He, and Hanghang Tong. 2025. Breaking Silos: Adaptive Model Fusion Unlocks Better Time Series Forecasting. *arXiv preprint arXiv:2505.18442* (2025).
- [23] Donghao Luo and Xue Wang. 2024. Modernctn: A modern pure convolution structure for general time series analysis. In *The twelfth international conference on learning representations*. 1–43.
- [24] Yuqi Nie, Nam H. Nguyen, Phanwadee Sinthong, and Jayant Kalagnanam. 2023. A Time Series is Worth 64 Words: Long-term Forecasting with Transformers. In *11th International Conference on Learning Representations, ICLR 2023*.
- [25] Kanghui Ning, Zijie Pan, Yu Liu, Yushan Jiang, James Yiming Zhang, Kashif Rasul, Anderson Schneider, Lintao Ma, Yuriy Nevmyvaka, and Dongjin Song. 2025. TS-RAG: Retrieval-Augmented Generation based Time Series Foundation Models are Stronger Zero-Shot Forecaster. *arXiv preprint arXiv:2503.07649* (2025).

- [26] Boris N. Oreshkin, Dmitri Carpov, Nicolas Chapados, and Yoshua Bengio. 2020. N-BEATS: Neural basis expansion analysis for interpretable time series forecasting. *arXiv preprint arXiv:1905.10437* (2020).
- [27] Xiangfei Qiu, Hanyin Cheng, Xingjian Wu, Jilin Hu, Chenjuan Guo, and Bin Yang. 2025. A Comprehensive Survey of Deep Learning for Multivariate Time Series Forecasting: A Channel Strategy Perspective. *arXiv preprint arXiv:2502.10721* (2025).
- [28] Xiangfei Qiu, Jilin Hu, Lekui Zhou, Xingjian Wu, Junyang Du, Buang Zhang, Chenjuan Guo, Aoying Zhou, Christian S. Jensen, Zhenli Sheng, and Bin Yang. 2024. TFB: Towards Comprehensive and Fair Benchmarking of Time Series Forecasting Methods. *Proceedings of the VLDB Endowment* (2024), 2363–2377. Issue 9.
- [29] Xiangfei Qiu, Xingjian Wu, Hanyin Cheng, Xvuyuan Liu, Chenjuan Guo, Jilin Hu, and Bin Yang. 2025. DBLoss: Decomposition-based Loss Function for Time Series Forecasting. *arXiv preprint arXiv:2510.23672* (2025).
- [30] Zezhi Shao, Fei Wang, Yongjun Xu, Wei Wei, Chengqing Yu, Zhao Zhang, Di Yao, Tao Sun, Guangyin Jin, Xin Cao, Gao Cong, Christian S. Jensen, and Xueqi Cheng. 2025. Exploring Progress in Multivariate Time Series Forecasting: Comprehensive Benchmarking and Heterogeneity Analysis. *IEEE Transactions on Knowledge and Data Engineering* (2025), 291–305. Issue 1.
- [31] Xiaoming Shi, Shiyu Wang, Yuqi Nie, Dianqi Li, Zhou Ye, Qingsong Wen, and Ming Jin. 2025. Time-MoE: Billion-Scale Time Series Foundation Models with Mixture of Experts. *arXiv preprint arXiv:2409.16040* (2025).
- [32] Yanru Sun, Zongxia Xie, Dongyue Chen, Emadeldeen Eldele, and Qinghua Hu. 2024. Hierarchical Classification Auxiliary Network for Time Series Forecasting. *arXiv preprint arXiv:2405.18975* (2024).
- [33] Peiwang Tang and Weitai Zhang. 2024. Unlocking the Power of Patch: Patch-Based MLP for Long-Term Time Series Forecasting. *arXiv preprint arXiv:2405.13575* (2024).
- [34] Luan Tran, Manh Nguyen, and Cyrus Shahabi. 2019. Representation learning for early sepsis prediction. In *2019 Computing in Cardiology (CinC)*. IEEE, 1–4.
- [35] Hao Wang, Licheng Pan, Zhichao Chen, Degui Yang, Sen Zhang, Yifei Yang, Xinggao Liu, Haoxuan Li, and Dacheng Tao. 2025. FreDF: Learning to Forecast in the Frequency Domain. *arXiv preprint arXiv:2402.02399* (2025).
- [36] Huiqiang Wang, Jian Peng, Feihu Huang, Jince Wang, Junhui Chen, and Yifei Xiao. 2023. MICN: Multi-scale Local and Global Context Modeling for Long-term Series Forecasting. In *11th International Conference on Learning Representations, ICLR 2023*.
- [37] Shiyu Wang, Jiawei Li, Xiaoming Shi, Zhou Ye, Baichuan Mo, Wenzhe Lin, Shengtong Ju, Zhixuan Chu, and Ming Jin. 2025. TimeMixer++: A General Time Series Pattern Machine for Universal Predictive Analysis. *arXiv preprint arXiv:2410.16032* (2025).
- [38] Shiyu Wang, Haixu Wu, Xiaoming Shi, Tengge Hu, Huakun Luo, Lintao Ma, James Y. Zhang, and Jun Zhou. 2024. TimeMixer: Decomposable Multiscale Mixing for Time Series Forecasting. *arXiv preprint arXiv:2405.14616* (2024).
- [39] Yuxuan Wang, Haixu Wu, Jiayang Dong, Yong Liu, Mingsheng Long, and Jianmin Wang. 2024. Deep Time Series Models: A Comprehensive Survey and Benchmark. *arXiv preprint arXiv:2407.13278* (2024).
- [40] Yuxuan Wang, Haixu Wu, Jiayang Dong, Guo Qin, Haoran Zhang, Yong Liu, Yunzhong Qiu, Jianmin Wang, and Mingsheng Long. 2024. TimeXer: Empowering Transformers for Time Series Forecasting with Exogenous Variables. *arXiv preprint arXiv:2402.19072* (2024).
- [41] Kaimin Wei, Tianqi Li, Feiran Huang, Jinpeng Chen, and Zefan He. 2022. Cancer classification with data augmentation based on generative adversarial networks. *Frontiers of Computer Science* 16, 2 (2022), 162601.
- [42] Gerald Woo, Chenghao Liu, Akshat Kumar, Caiming Xiong, Silvio Savarese, and Doyen Sahoo. 2024. Unified training of universal time series forecasting transformers. In *ICML '24: Proceedings of the 41st International Conference on Machine Learning*.
- [43] Haixu Wu, Tengge Hu, Yong Liu, Hang Zhou, Jianmin Wang, and Mingsheng Long. 2023. TimesNet: Temporal 2D-Variation Modeling for General Time Series Analysis. In *11th International Conference on Learning Representations, ICLR 2023*.
- [44] Haixu Wu, Jiehui Xu, Jianmin Wang, and Mingsheng Long. 2021. Autoformer: Decomposition transformers with auto-correlation for long-term series forecasting. *Advances in neural information processing systems* 34 (2021), 22419–22430.
- [45] Haixu Wu, Hang Zhou, Mingsheng Long, and Jianmin Wang. 2023. Interpretable weather forecasting for worldwide stations with a unified deep model. *Nature Machine Intelligence* (2023), 602–611. Issue 6.
- [46] Haonan Yang, Jianchao Tang, Zhuo Li, and Long Lan. 2025. DMSC: Dynamic Multi-Scale Coordination Framework for Time Series Forecasting. *arXiv preprint arXiv:2508.02753* (2025).
- [47] Kun Yi, Qi Zhang, Wei Fan, Shoujin Wang, Pengyang Wang, Hui He, Ning An, Defu Lian, Longbing Cao, and Zhendong Niu. 2023. Frequency-domain MLPs are more effective learners in time series forecasting. *Advances in Neural Information Processing Systems* 36 (2023), 76656–76679.
- [48] Xinli Yu, Zheng Chen, Yuan Ling, Shujing Dong, Zongyi Liu, and Yanbin Lu. 2023. Temporal Data Meets LLM – Explainable Financial Time Series Forecasting. *arXiv preprint arXiv:2306.11025* (2023).
- [49] Ailing Zeng, Muxi Chen, Lei Zhang, and Qiang Xu. 2023. Are transformers effective for time series forecasting?. In *Proceedings of the AAAI conference on artificial intelligence*, Vol. 37. 11121–11128.
- [50] Haoyi Zhou, Shanghang Zhang, Jieqi Peng, Shuai Zhang, Jianxin Li, Hui Xiong, and Wancai Zhang. 2021. Informer: Beyond efficient transformer for long sequence time-series forecasting. In *Proceedings of the AAAI conference on artificial intelligence*, Vol. 35. 11106–11115.